International Journal for Multidisciplinary Research (IJFMR)
E-ISSN: 2582-2160 ● Website: www.ijfmr.com ● Email: editor@ijfmr.com

Road Perception and Detection Technology Based on Line Structured Light

Jerome Ofori-Kyeremeh[1], Prof. Li Feng[2], Kingsley Ofori[3], Richmond Yeboah[4], Victor Twene Dapaah[5]

[1,5]Senior Teacher, Basic School, University of Energy and Natural Resources
[2]Lecturer, School of Electronics and Information, Jiangsu University of Science and Technology
[3]Teacher, Mathematics and Computing, Ghana Education Service
[4]Teacher, Basic School, University of Energy and Natural Resources

ABSTRACT

Line structured light is one of the most active research areas in Computer Vision and Image Processing and has been extensively studied in recent years. Line structured light has a wide application prospects in industry for dimensional analysis, on-line inspection, component quality, and reverse engineering, due to its simplest structure, moderate accuracy and fast speed.

Over the decades, road perception and detection technology has been focusing on LiDAR, which has hampered its full implementation, aside the numerous benefits of the technology. This research work looks at how to use line structured light instead of LiDAR in road perception and detection technology. Drawing inference from the research, it was concluded that the proposed technology on road perception and detection is better over LiDAR in foggy and dusty condition aside the high cost of LiDAR, when compared.

Keywords: Computer Vision, Image Processing, Road Perception and Detection, Road Obstacle Detection and Autonomous Vehicle.

INTRODUCTION

Road perception is the autonomous system's capacity to gather the information it needs from its surroundings, extract pertinent information, and create a contextual awareness of its surroundings, including the location of obstacles and the recognition of road signs or markings. Besides, the autonomous car uses localization to figure out where it is in relation to its surroundings. Autonomous vehicles receive vital information about the driving environment, such as the free driving area around obstacles and their velocities, using road perception. While there are some conventional methods for detecting road obstacles that use ultrasonic sensors and short- or long-range radars, line-structured light was used in this research [1]. Road obstacle detection is an extensively researched domain in the automotive sector due to its critical significance in all systems facilitating autonomous vehicle navigation within the surroundings. Numerous road obstacle detection systems have been created over the years, with the primary distinctions among them being the algorithms and sensors utilized. A multitude of studies has concentrated on road obstacle identification to facilitate tasks such as pre-collision, obstacle evasion, and inter-distance regulation. In the roadway context, any surface elevated above the ground is regarded as an impediment [2]. Road

impediments result in significant accidents that adversely affect driver safety, traffic flow efficiency, and vehicle integrity.

Road obstacle detection is crucial for preventing or minimizing these types of collisions and fatalities [3]. Road obstacle identification is challenging because of the variety of the obstacle elements, which include varying sizes, shapes, colors, and positions, none of which can be predicted in advance. However, dust and fog can readily overcome passive sensors like cameras, but they can negatively impact active sensors like LiDAR, radar, sonar, and infrared. Once more, it is time for the system to respond and detect things reliably [4].

LIDAR

Light Detection and Ranging, or LiDAR, is a device that functions similarly to radar but uses infrared light pulses which are invisible to the human eye in the form of lasers instead of radio waves. It then calculates how long it takes for the pulses to return after striking an obstacle. It does this millions of times in every second, it compiles the results into a so called point cloud, which functions in real time like a three-dimensional map of the globe. The map is so thorough that it can be used to identify objects in addition to simply spotting them. LiDAR detection techniques generally fall into two categories: coherent detection and direct energy detection, commonly referred to as incoherent detection. Doppler or phase-sensitive measurements work best with coherent systems. However, for wind measurement, the direct energy detection transforms the doppler frequency shift into an intensity change or intensity spatial distribution. If the necessary spectrum information is provided, the direct energy detection system can measure both temperature and wind. Although this enables them to function at significantly less power, it comes at the cost of more intricate transceiver specifications. Lasers, scanners and optics, photodetector and receiver electronics, and navigation and position systems are the four (4) primary parts of the LiDAR systems. The latter, which involves installing a LiDAR sensor on a mobile platform like satellites, aircraft, or cars in order to ascertain an object's exact location, will receive more attention for the purposes of this research than the former. In addition to being utilized in autonomous vehicles to detect obstacles, LiDAR is widely used in robotics to help robots identify the best routes to avoid natural dangers. Since autonomous vehicles are seen to have the ability to provide benefits including improved road efficiency, enhanced productivity, greater accessibility, and environmental benefits, they must play a significant part in the urban transportation system. Only with appropriate road perception and detecting technology can this vision could be achieved.

Autonomous vehicle systems have significantly improved over time due to the availability of computing technology and have drawn more attention from academics. Google created and tested a variety of autonomous car models using advanced LiDAR on the road in 2009. Google discovered that the LiDAR they utilized in their systems had limitations in the areas in which it operated, and that the cost was still another difficult problem that prevented them from using it.

A lot of research have been conducted on LiDAR as an obstacle detection tool, and the general consensus is that it is difficult to detect obstacles in foggy conditions, is impacted by dust, and is expensive (because to its expansiveness). These LiDAR flaws make it challenging to precisely determine how much distance an autonomous car needs to pass in order to avoid colliding. The main problem with road perception and detection technology is figuring out what the world is like by using a camera or sensor to record and process sensory inputs. Since the extracted information is the same information that the system utilizes to comprehend its surroundings and take appropriate action. The use of passive sensors for perception has

numerous justifications. Among other reasons, precision, adaptability, and dependability are frequently mentioned. Furthermore, a substantial amount of academic study has been done on the use of LiDAR for obstacle detection and avoidance by a variety of researchers. However, it has only recently been proposed to use line-structured lights for road perception and detection. This research serve as the basis for line-structured light technology used in road perception and detection. In the end, line-structured light is the greatest option over alternatives like LiDAR since it uses a variety of light stripes to identify different kinds and sizes of obstacles [5].

STRUCTURED LIGHT

A thorough and prompt vision inspection depends heavily on the lighting's suitability and quality. The topic of structured light is fundamental to almost every field of study and industry, including stereo vision, conventional space two-dimensional (2-D) and three-dimensional (3-D) modeling, and product inspection. Lighting quality and suitability are essential for its use, and a detailed examination of the inspection area is required to obtain an efficient vision system. An active optical approach, which uses one or more light sources and one or more cameras for shape acquisition, is used to measure the surface of an object. They are currently widely utilized in a variety of fields, including robotics, machines, computer games, meterology, and more. Recent advancements in computing power and sensor technology have made them more precise, quick, and adaptable enough for widespread application. The first structured light system, the launch of the Microsoft Kinect 1 single-shot structured light system, the creation of the Photon Mixer Device (PMD) for Time of Flight imaging, and the availability of extremely accurate systems from manufacturers such as GOM, Hexagon metrology, and Aicon 3-D system were crucial to this development. Over the years, numerous researchers have developed a variety of unique active optical sensor acquisition techniques. These can be divided into two (2) primary groups: range sensors that provide high-precision range maps at a rate of over 100 frames per second through the use of dynamic triangulation. In order to locate the laser, this category uses the sensory attention paradigm in each row. The last category uses visual disparity and triangulation based on the sensors. Because of its versatility, speed, accuracy, non-contact nature, and affordability, structured light has emerged as a popular modality for optical form capture. There are three (3) types of structured light: single line structured light, multiple line structured light, and projector type. Structured light is important for visual sensing in various applications. The reason for which structured light is employed determines which category is adopted. For example, a single line structured light is used for surface inspection and steam tracking measurements, and its implementation in practice is due to its handling and affordability. The projector type is used when stripes of lines are required and users choose a specific design [6]. Multiple line structured lights are used when more measurement information is required. Materials with less-than-ideal optical qualities present the biggest obstacle in structured light, whether it be for precise measurement or head tracking.

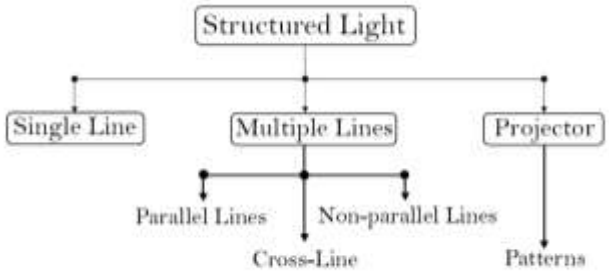

Figure 1 categories of structured light

STRUCTURED LIGHT LINE TECHNOLOGY

Structured light falls into the following categories: triangulation-based, reflecting, non-contact, and optically active. Considering all 3-D optical surface measurement methods, structured light technology has been researched the most over the past ten years because of its benefits, which include high-speed, high-resolution measurement and system flexibility. The accuracy of structured light technology is mostly dependent on the method used for system calibration, which calls for precise calibration of both the active illumination and picture acquisition devices. The most crucial aspect of structured light that requires careful thought is the precise and accurate calibration of the projector and camera, or intrinsic parameters, as well as the spatial relationship between them, or extrinsic parameters. Treating the projector as an inverse camera is a popular calibration technique that provides a higher degree of precision [7]. A camera, projector, object, and processing unit (computer) make up the most basic structured light system. In order to determine the 3-D shape of the object through triangulation, the computer executes the decoding algorithm to extract the necessary coordinated information from the scanned object that connects the camera and projector coordinates. Since coding and decoding algorithms determine the ultimate quality of the item, the most crucial factor in accuracy is once again how to create the projected patterns, or how to construct the different techniques for coding and decoding algorithms. In the decade leading up to 2025, numerous structured light systems have been developed, and research on how to create a strong structured light system that can specifically recognize patterns on a scene is still underway in the structured light literature [8]. As at now, no ideal pattern scheme for structured light has been developed, and most of the structured light solutions that have been suggested in the past are still being researched. Numerous classifications for various coding schemes have been proposed using the characteristics of patterns [9]. While there are dot and line patterns when the light source is a laser, the projected patterns are primarily a collection of well-designed 2-D images. 2-D image pattern techniques are always favored for quick scanning when employing a digital light processing (DLP) or digital micro mirror device (DMD) projector as the light source. The two types of 2-D pattern classifications are one shot and multi-shot schemes are generally used where 2-D pattern strategies lie, despite the fact that, numerous ways have been created and its resilience to motion, one-shot patterns suffer from errors and greater computing costs [10].

LINE STRUCTURED LIGHT

Projecting a predefined pattern onto a scene typically grids or horizontal bar is known as line structured light. The basic principle behind this method is that, like in structured light 3-D scanners, vision systems can determine the depth and surface information of objects in a scene by using line-structured light after impacting surfaces. Because the patterns are projected onto the object (like in classical photogrammetry), line-structured light also provides a description of discrete object coordinates, resulting in excellent accuracy on well-defined object/image properties like edges and texture. Because of its straightforward design, moderate precision, and quick speed, the line-structured light has a wide range of industrial applications for dimensional analysis, online inspection, component quality, and reverse engineering [11, 12]. The calibration of the light plane equation and camera calibration are the two processes that make up the parameters calibration for line structured light.

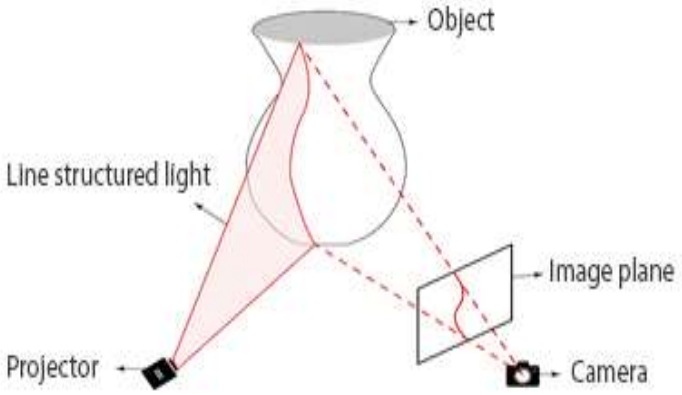

Figure 2 projection of line structured light

From figure 2, projector was used to project line-structured light onto an object's surface. The projector's light was detected by the object's shape, which causes the light to reflect the object's shape. The shape is then captured in the image plane by the camera.

LINE STRUCTURED LIGHT VISION MODEL

The line structured light vision sensor is composed of a laser projector and a camera. The camera captures the image of the laser profile that is the intersection line of the laser plane.

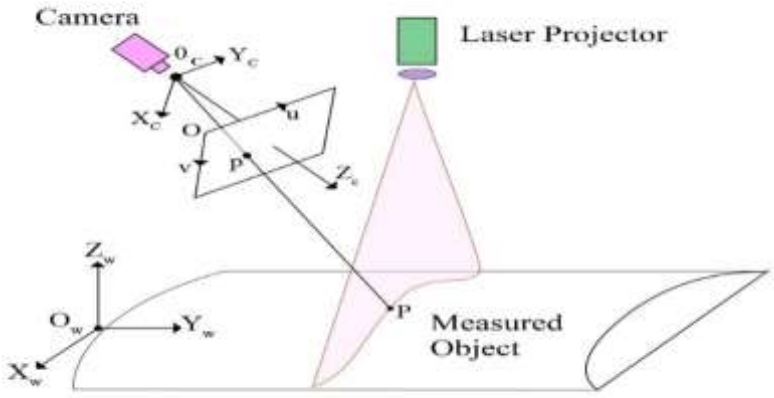

Figure 3 schema of the line structured light vision model

Calculating the laser profile's three-dimensional coordinates is the task of line-structured light vision. As seen in the above figure 3, the camera coordinate frame (CCF) *Oc, Xc, Yc*, and *Zc* is typically used to measure the 3-D coordinate system. The lens's optical center is denoted by *Oc*, and its optical axis is denoted by *OcZc*. The imaging plane's horizontal line and vertical line are denoted by the axes *OcXc* and *OcYc*, respectively. Again the image coordinate frame (ICF) is based on the *O-uv* picture that was taken by the camera. ICF is measured in pixels.

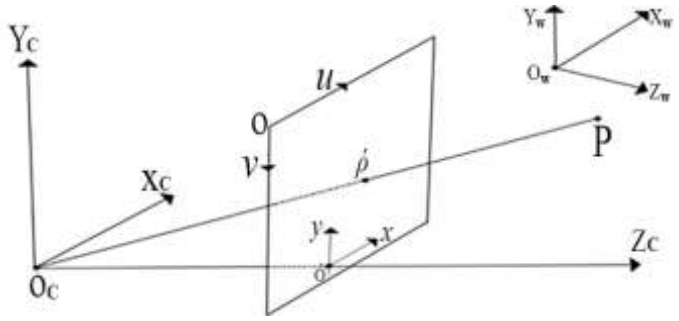

Figure 4 coordinate system analysis diagram

The coordinates of the space point P are Pc (Xc, Yc, Zc) in the camera coordinate frame and P (Xw, Yw, Zw) in the world coordinate frame. A translation matrix T and a rotation matrix R are used to achieve the transformation between the two coordinate frames. As can be seen, R is a 3x3 moment matrix and T is a 1x3 matrix as shown in equation matrix as shown in equation 1.1

$$\begin{bmatrix} X_c \\ Y_c \\ z_c \end{bmatrix} = R \begin{bmatrix} X_w \\ Y_w \\ z_w \end{bmatrix} + T \qquad (1.1)$$

The equation 1.1 is further transform into homogeneous matrix

$$\begin{bmatrix} X_c \\ Y_c \\ z_c \\ 1 \end{bmatrix} = \begin{bmatrix} R & 0 \\ 0 & 0 \end{bmatrix} \begin{bmatrix} X_w \\ Y_w \\ z_w \\ 1 \end{bmatrix} + \begin{bmatrix} T \\ 0 \end{bmatrix} = \begin{bmatrix} R & T \\ 0 & 0 \end{bmatrix} \begin{bmatrix} X_w \\ Y_w \\ z_w \\ 1 \end{bmatrix} \qquad (1.2)$$

Equation 1.2 can also be further written as

$$z_c \begin{bmatrix} X \\ Y \\ 1 \end{bmatrix} = \begin{bmatrix} f_c & 0 & 0 & 0 \\ 0 & f_c & 0 & 0 \\ 0 & 0 & 1 & 0 \end{bmatrix} \begin{bmatrix} X_c \\ Y_c \\ z_c \\ 1 \end{bmatrix} \qquad (1.3)$$

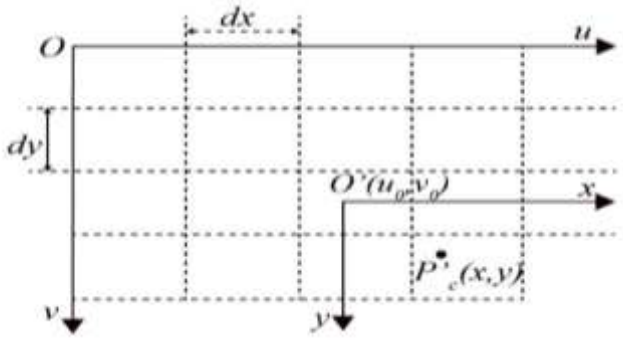

Figure 4 physical coordinate system and the image pixel coordinate system

Each grid in the picture represents an image. The point $O'(u_o, v_o)$ is the origin of the physical coordinate system, *dx* and *dy* represent the image pixel system.

$$\begin{cases} u = \frac{x}{dx} + u_0 \\ v = \frac{y}{dy} + v_0 \end{cases} \qquad (1.4)$$

The image physical coordinates mentioned above are the coordinates in ideal state but because of the distortion of optical lens, the distortion of the actual image coordinates are smaller than that of the ideal image physical coordinates. Using distortion γ'equation 1.4 can further be written as;

$$\begin{bmatrix} u \\ v \\ 1 \end{bmatrix} = \begin{bmatrix} 1/dx & \gamma' & u_0 \\ 0 & 1/d_y & v_0 \\ 0 & 0 & 1 \end{bmatrix} \begin{bmatrix} X \\ Y \\ 1 \end{bmatrix} \quad (1.5)$$

Equations (1.3) and (1.5) combined to get a conversion formula from image pixel coordinate system to world coordinate system.

$$z_c \begin{bmatrix} u \\ v \\ 1 \end{bmatrix} = \begin{bmatrix} 1/dx & \gamma' & u_0 \\ 0 & 1/d_y & v_0 \\ 0 & 0 & 1 \end{bmatrix} \begin{bmatrix} f_c & 0 & 0 & 0 \\ 0 & f_c & 0 & 0 \\ 0 & 0 & 1 & 0 \end{bmatrix} \begin{bmatrix} R & T \\ 0 & 0 \end{bmatrix} \begin{bmatrix} X_w \\ Y_w \\ z_w \\ 1 \end{bmatrix} \quad (1.6)$$

$$z_c \begin{bmatrix} u \\ v \\ 1 \end{bmatrix} \begin{bmatrix} a_u & \gamma' & u_0 \\ 0 & a_v & v_0 \\ 0 & 0 & 1 \end{bmatrix} [RT] \begin{bmatrix} X_w \\ Y_w \\ z_w \\ 1 \end{bmatrix} \quad (1.7)$$

Where a_u the scale factor on u for the image, a_v the scale factor on v . From the above, γ' can also be expressed as follows:

$$A = \begin{bmatrix} a_u & \gamma' & u_0 \\ 0 & a_v & v_0 \\ 0 & 0 & 1 \end{bmatrix} \quad (1.8)$$

Equation 1.7 can be simplified as;

$$\lambda P_{uv} = A[\ R\ \ T\ ]P_w \quad (1.9)$$

Where A is the camera intrinsic matrix, λ is the arbitrary scaling factor, P_{uv} is the coordinates of the principal point, P_w is a point in the world coordinate system, and (RT) is the extrinsic parameters, which are the rotation and translation that connect the world coordinate system to the camera coordinate system.

CAMERA CALIBRATION

In computer vision, where jobs frequently entail the computation of precise quantitative measurements from images, camera calibration is an essential concern. Three-dimensional geometric interpretation of images is impossible without camera calibration. Using a variety of existing algorithms for three-dimensional (3-D) reconstruction and recognition, all of which rely on the camera parameters, is made possible by efficient camera calibration techniques. Finding the precise transformation that converts a scene's 3-D points into their matching 2-D projections onto the camera's image plane is made easier with camera calibration. This operation involves estimating two sets of parameters: the intrinsic (or internal) parameters that characterize the camera's internal geometry, and the extrinsic (or external) parameters that define the camera's pose, or location and orientation in space. Zhang Zhengyou's plane calibration approach was adopted in this research because it is more accurate than the self-calibration method [13]. In order to retrieve the camera settings, the calibration board was moved to take calibration photographs at various positions. The computer then recorded the image and analyzed it using Matlab. Zw = 0 when the calibration plate's plane is viewed as the O-XY plane of the global coordinate system. The following

represents the conversion relationship between the world coordinate system and the pixel coordinate system

$$z_C \begin{bmatrix} u \\ v \\ 1 \end{bmatrix} = A[r_1 r_2 r_3 T] \begin{bmatrix} X_w \\ Y_w \\ z_w \\ 1 \end{bmatrix} = A[r_1 r_2 T] = H \begin{bmatrix} X_w \\ Y_w \\ 1 \end{bmatrix} \quad (1.10)$$

Where z_C is the scaling factor, $r_1 r_2 r_3$ is the column vectors of the rotation matrix *R*, *T* is the translation matrix. From the above equation 3.10, *H* can be express as a column-matrix form, as follows;

$$H = [\mathrm{h_1 h_2 h_3}] = \lambda[r_1 r_2 \mathrm{T}] \quad (1.11)$$

Where λ is an arbitrary scalar, $r_1 r_2$ is the first and second columns of orthogonal rotation matrix *R*. *T* is the translation matrix. By the nature of orthogonal matrix, we have;

$$r_1^T r_1 = 1,\ r_2^T r_2 = 1 \text{ and } r_1^T r_2 = 0 \quad (1.12)$$

Where *T* denotes matrix transposition and from Equation (1.10) and (1.11), we have;

$$h_1{}^{\mathrm{T}} A^{-\mathrm{T}} A^{-1} h_2 = 0 \quad (1.13)$$

$$h_1{}^{\mathrm{T}} A^{-\mathrm{T}} A^{-1} h_1 = h_2{}^{\mathrm{T}} A^{-\mathrm{T}} A^{-1} h_2 \quad (1.14)$$

The extrinsic matrix can be obtained by the result of *A* which is the camera intrinsic parameter and Equation (1.12) as follows;

$$r_1 = \lambda A^{-1} h_1$$
$$r_2 = \lambda A^{-1} h_2 \quad (1.15)$$
$$r_3 = r_1 x r_2$$
$$T = \lambda A^{-1} h_3$$

Where $\lambda = 1/\|A^{-1}h_1\| = 1/\|A^{-1}h_2\|$

Furthermore, we consider lens distortion, which can be express as;

$$u_d = u + k_1 u(u^2 + v^2) + k_2 u(u^2 + v^2)^2 \quad (1.16)$$
$$v_d = v + k_1 v(u^2 + v^2) + k_2 v(u^2 + v^2)^2$$

Where (u, v) and (u_d, v_d) are the ideal pixel image coordinates and the real image coordinates respectively. k_1, k_2 are coefficients of radial distortion. Then, the optimal solution with radial distortion can be calculated. The objective function for optimization is defined as;

$$\sum_{i=1}^{n} \sum_{j=1}^{m} \|P_{ij} - \hat{P}(A, R_i, T_i, u_{d_{i_j}}, v_{d_{i_j}}, k_1, k_2)\| \quad (1.17)$$

Where P_{ij} is the actual coordinates of the *j*-th point in *i*-th image, $(u_{d_{i_j}}, v_{d_{i_j}})$ are the pixel image coordinates , $\hat{P}(A, R_i, T_i, u_{d_{i_j}}, v_{d_{i_j}}, k_1, k_2)$ is the calculation result of coordinates, *n* denotes the total number of images and *m* denotes the number of points in each image.

CALIBRATION OF LINE STRUCTURED LIGHT

To determine the relationship between the camera and the light plane projector, the line structured light must be calibrated. Finding the light plane's normal vector and determining the light plane's distance parameter are two crucial factors that must be properly taken into account during the line structured light calibration process. A camera and a light plane projector make up the line structured light, and once the system is configured, the relationship between the two is fixed. The light plane projection does not alter during the calibrating process.

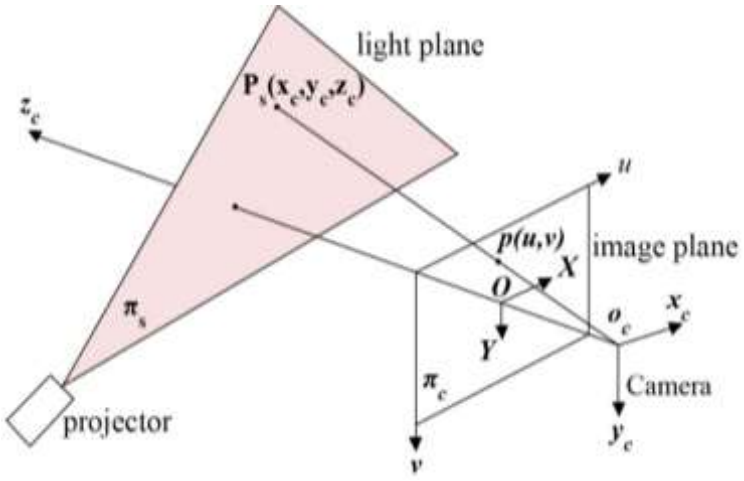

Figure 5 measurement model of line structured light

According to the model's above illustration, the camera coordinate frame is oc,xc,yc,zc. OXY represents the image coordinate frame in millimeters, and O-uv represents the image coordinate frame in pixels. With the perspective projection model in mind the equation between the point $P = (x_c\ y_c\ z_c)^T$ in the camera coordinate frame and its image coordinate $P = (u, v)^T$

$$s\begin{bmatrix}u\\v\\1\end{bmatrix} = K\begin{bmatrix}a_x & \gamma & u_0\\0 & a_y & v_0\\0 & 0 & 1\end{bmatrix} \qquad (1.18)$$

Where $K\begin{bmatrix}a_x & \gamma & u_0\\0 & a_y & v_0\\0 & 0 & 1\end{bmatrix}$ the intrinsic parameter of the camera obtained by the camera calibration, γ indicates the skewness of the two picture axes, s is the arbitrary unknown scaler, a_x and a_y are the camera's effective focal lengths, and ,(u_0,v_0) is the primary point. Once more, let P be an ideal projection point in the image plane π_c.and P_s be an arbitrary point in the light plane π_s the intersection of the projection from o_cp and πs is then the arbitrary point P_s. The three-dimensional (3-D) position of the observed point P_s is expressed as follows using the equation of the light plane πs and the line equation of o_cp, which is in the camera coordinate frame:

P_s that is been measured is written as follows;

$$s\begin{bmatrix}u\\v\\1\end{bmatrix} = K\begin{bmatrix}x_c\\y_c\\z_c\end{bmatrix} \qquad (1.19)$$

$$a_cx_c + b_cy_c + c_cz_c + d_c = 0$$

Where, normal vector of the light plane $n_c = (a_c, b_c, c_c)^T$ and d_c is the parameter of the light plane. The vanishing line l of a plane π in a three-dimensional (3-D) space is determined by l'_0, l'_1, l'_2 , which are the images of three coplanar with equally spaced parallel straight line[14] then the following equation holds:

$$l = (l'_0 \times l'_2)^{\mathrm{T}}(l'_1 \times l'_2)l'_1 + 2(l'_0 \times l'_1)^{\mathrm{T}}(l'_2 \times l'_1)l'_2 \qquad (1.20)$$

3-DIMENSIONAL DATA POINT EXTRACTION USING LINE PATTERNS

In figure 6 below, a projector projects line patterns onto an object from a computer. The projected line pattern is reflected by the surface of the item; the camera then records the shape the line pattern creates with the object and stores the image for later processing. One important consideration that requires careful

consideration is that, when taking these pictures, the camera should only record one type of line pattern in each picture.

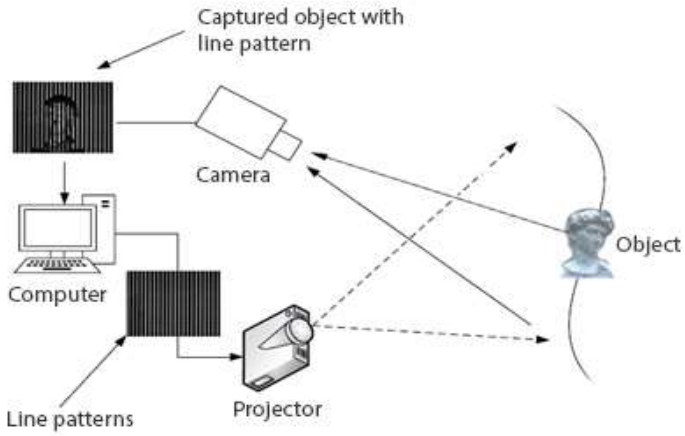

Figure 6 schematic representation of the system configuration layout

The line pattern to be projected was created using the Matlab software. The mode of the projector is set to black and white (B/W) to avoid the image's outcome being impacted by the object's surface color.

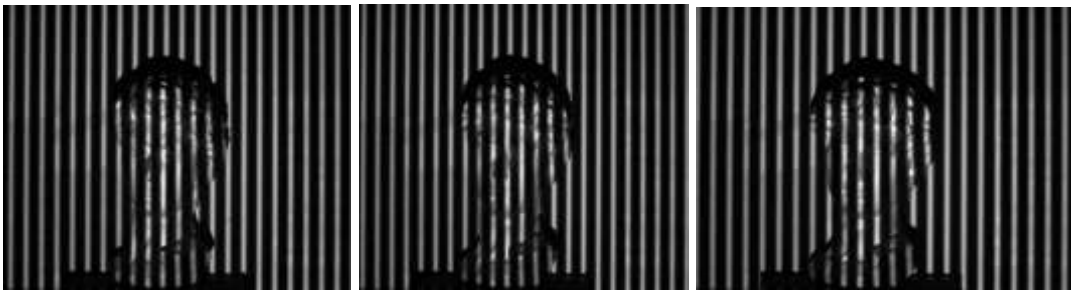

(a) (b) (c)

Figure 8 projection of line patterns from the projector unto an object

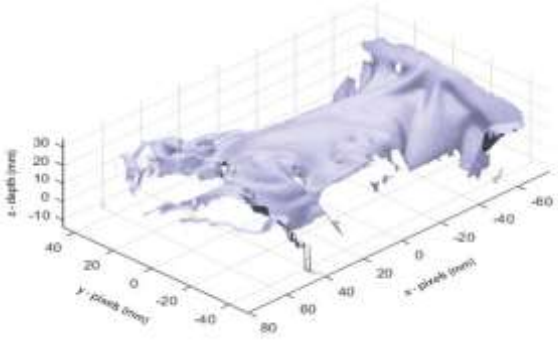

Figure 9 result of 3-D data point extraction

CAMERA CALIBRATION RESULTS

Following the calibration of nine (9) checkerboard images using Zhang Zhengyou's method of camera calibration, the reprojection error by [15] is displayed in figure 10 below. In contrast to the overall mean pixel error of 0.13 pixels in figure 11, the overall mean pixel error in their work was 0.90 pixels. The calibration's accuracy is shown in the bar graph. The mean reprojection error for the associated calibrated

image is displayed by each bar. The difference between the corner points found in the image and the matching ideal world points projected into the image is known as the reprojection errors. Examine carefully the reprojection error of the calibrated pictures in figures 10 and 11 below. In contrast to the overall mean error of 0.90 pixels from the calibration procedure outlined by [15] utilizing 9 checkerboard images, the calibration findings of 30 checkerboard images in this study had an overall mean error of 0.13 pixels. Pixel mistake happens when one or more pixels in a frame don't accurately reflect the data that was taken. According to the aforementioned study, it is preferable to employ more checkerboard images for the calibration in order to have a smaller overall mean error of pixels reprojection. (for example, 30 images instead of 9).

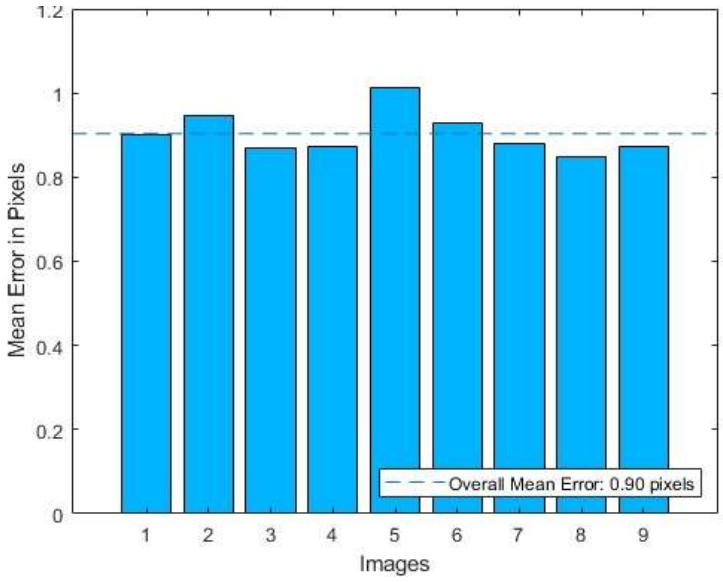

Figure 10 Reprojection error by Mathworks

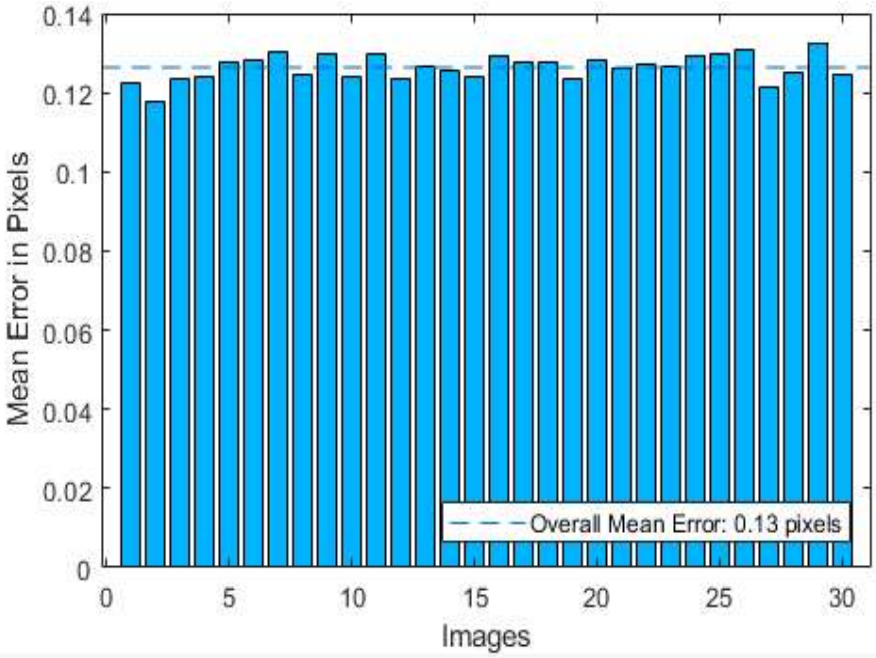

Figure 11 Reprojection error

The amount of checkerboard pictures utilized for the camera calibration is the reason for the 0.77 variation in the total mean error of pixels reprojection between figures 10 and 11According to mathematics, the number of calibrated images are inversely proportional to the total mean error pixel, as determined by the Zhang technique [13]. A 1292x964 Manta G-125C camera with the intrinsic parameters ax = 0.0044455, ay = 0.0044419, u_0 = 655.3002, v_0 = 397.5046, γ = 0, k1 = -0.1532, and k2 = 0.6620. Since γ is zero (0), it is usually insignificant in this study activity, but according to [16], it is frequently used to account for the fact that the two axes in the sensor lattice are not completely perpendicular. The checkerboard and the camera are roughly 60 meters apart.

CENTRE LINE EXTRACTION RESULTS

By analyzing figure 5, the equation of the line in the image coordinate system was obtained. The points' coordinates were taken out of the two linear equations. The camera matrix transformation was used to determine the coordinates of the locations in the world coordinate system. The space plane equation is established since a plane is uniquely determined by the non-collinear points in space. The coordinates of the points are used to set the equation under a known circumstance. Solving the acquired light plane equation yields the coefficient of the space plane equation.

Let the equation of the line plane be the same as that of an empty space then;

$$A_x + B_y + C_z + D = 0 \qquad (1.21)$$

The coordinates of the points extracted in the image coordinate system are;

$$P_{1_i} = (x_{1_i}, y_{1_i}, 1)^T \qquad (1.22)$$

Where i= 1, 2, 3 the coordinates of the points in the space coordinates system obtained by the camera matrix transformation then becomes as follows;

$$P_{c_i} = (x_{c_i}, y_{c_i}, z_{c_i}, 1)^T \qquad (1.23)$$ i= 1, 2, 3 then $P_1 = \boldsymbol{H}P_c$

The following equation is established

$$\begin{bmatrix} x_{c_1} & y_{c_1} & z_{c_1} & 1 \\ x_{c_2} & y_{c_2} & z_{c_2} & 1 \\ x_{c_3} & y_{c_3} & z_{c_3} & 1 \end{bmatrix} \begin{bmatrix} A \\ B \\ C \\ D \end{bmatrix} = \begin{bmatrix} 0 \\ 0 \\ 0 \\ 0 \end{bmatrix} \qquad (1.24)$$

From the equation (1.24) above, the coefficient of the space plane equation is; A_0, B_0, C_0, D_0

The light plane equation then becomes;

$$A_0x + B_0y + C_0z + D_0 = 0 \qquad (1.25)$$

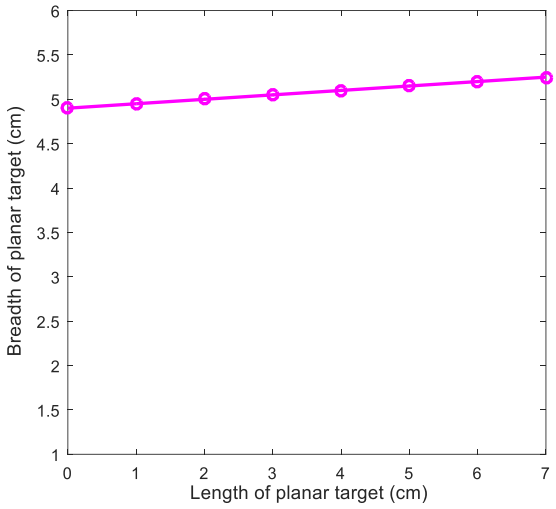

(a)

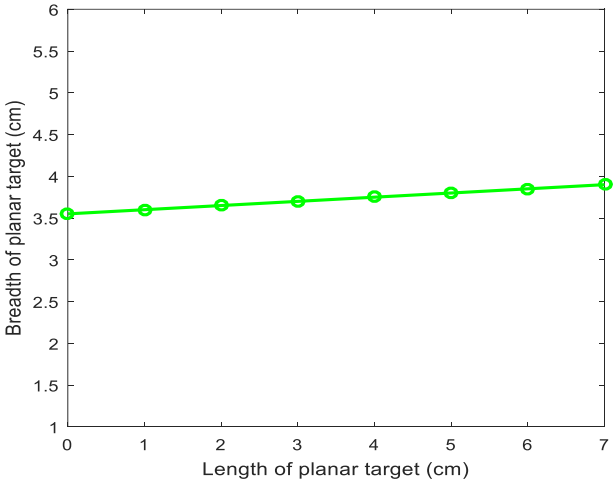

(b)

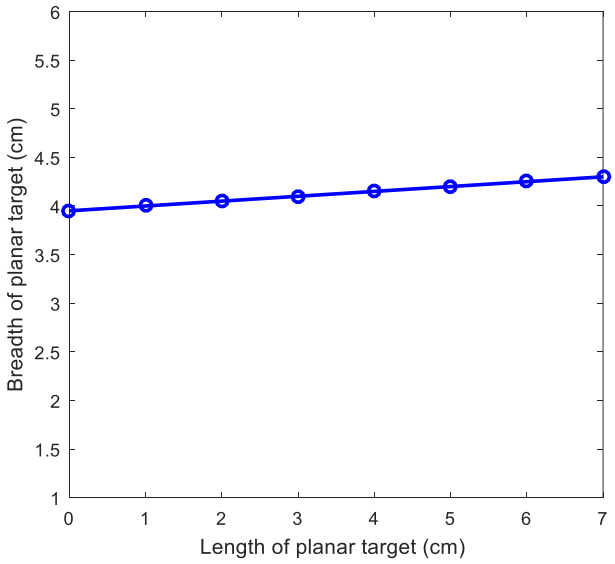

(c)

Figure 12 results of centre line extraction

REGION OF INTEREST (ROI) EXTRACTION RESULTS

There are several impediments on the road, and in order to prevent head-on collisions, these obstacles must be identified and dealt with. To improve identification time and speed, it is usually recommended to use region of interest to find an obstacle. Rapidly identifying the ROI and then focusing image processing using the ROI-selected image as a reference point is perfect and crucial for lowering computing complexity and enhancing image processing performance. With the suggested technology, the autonomous vehicle will have a clear picture of the free driving space surrounding the obstacle, its position, its velocity, and its shape once the ROI has been chosen. The autonomous vehicle uses the chosen ROI as its point of reference. In this research, the ROI was extracted using object-based technique. Since the object-based technique gives global information about the targets, including their size, shape, structure, and appearance [17]. Also, it is critical to remember that the ROI that is extracted is what is used for edge detection and subsequent processing.

EDGE DETECTION RESULTS

Road edge detection is crucial because the features that are extracted aid in determining the precise location, size, and speed of road impediments as well as the direction of the road extension. This will let the autonomous vehicle recognize which obstacles to avoid and determine whether it is outside its designated driving zone. Sobel operator was chosen and applied to identify the edges of the ROI-extracted image in this research ahead of other operators, such as the Canny operator, Robert operator, and Laplace filter because Sobel operator emphasizes the image's edges, produces the same result each time it runs over an image, and is rapid to run without requiring human involvement [18]. The 3-D data points are extracted from the edge-detected images. The data points are utilized to describe the image's structure and to visualize the images. Once more, it provides visibility distance estimation that is, the maximum geometric distance along the road's pathway.

CONCLUSION

Road obstacles lead to major accidents that seriously affect car damage, traffic flow efficiency and driver safety. Obstacle detection is crucial to preventing or minimizing these types of mishaps and fatalities. Numerous research have been done on LiDAR's ability to detect impediments, and the general consensus is that it is difficult to utilize in foggy environments, expensive due to its expansiveness, and impacted by dust. These LiDAR flaws make it challenging to precisely determine how much room an autonomous car needs to pass in order to avoid colliding. This study proposes road perception and detection technology based on line-structured light. In order to decrease traffic accidents, the suggested technology gives the autonomous system pertinent information about their surroundings, such as the places that are safe for driving around obstacles. The initial step in road perception and detection technology based on line structured light is to calibrate the camera and line structured light. Understanding the distortion coefficients and intrinsic and extrinsic characteristics is aided by camera calibration. While the extrinsic parameter also addresses the camera's position in reference to a fixed object, the intrinsic parameter deals with the focal length, optical center, lens distortion coefficients, and pixel-scaling factor. Calibration creates the connection between the camera and the laser projector while the light is line-structured. The points within the obstacles are extracted using line-structured light technology. Following the extraction of these points, the image's ROI is calculated to lengthen processing and calculation times, and the image's edges are identified to preserve its structural integrity. Again, visibility distance estimation was obtained

by extracting three-dimensional (3-D) data points. Lastly, based on the Matlab experimental results and conclusions from this study, it is determined that, despite LiDAR's expensive cost, the suggested technology for road perception and identification performs better than LiDAR in foggy and dusty conditions.

FUTURE WORKS

With the suggested technology, the research focused mostly on the software component and the processes involved, paying little attention to the hardware or how the software and hardware would be integrated. Once more, the experiment was carried out on a platform that was immobile. It is necessary to carry out additional study on how to include the suggested technology into a mobile platform and how the collected data is converted into three-dimensional (3-D) figures. This should be the focus of contemporary research projects.

REFERENCES

1. A. Asvadi, C. Premebida and P. Peixoto "3D Lidar-based static and moving obstacle detection in driving environments: An approach based on voxels and multi-region ground planes," Rob. Auton. Syst., 2016;83:299–311.
2. R. Manduchi, A. Castano and A . Talukder "Obstacle Detection and Terrain Classification for Autonomous Off-Road Navigation," 2015: 81–102.
3. V. R. Shah, S. V. Maru, and R. H. Jhaveri, "An Obstacle Detection Scheme for Vehicles in an Intelligent Transportation System," Int. J. Comput. Netw. Inf. Secur.,2016;8(10):23–28.
4. Z. Tianxu, P. Jiaxiong, and L. Zongjie, "An Adaptive Image Segmentation Method with Visual Nonlinearity Characteristics," 1996;26(4): 97–99.
5. H. Shao, K. Li, and Z. Zhang, "Study on Long-Distance Obstacle Perception of the Line Structured Light Sensor ," 2015: 357–362.
6. P. Kiddee, Z. Fang, and M. Tan, "Optik A practical and intuitive calibration technique for cross-line structured light," Opt. - Int. J. Light Electron Opt., 2016;127(20):9582–9602.
7. V. Suresh, J. Holton, and B. Li, "Structured light system calibration with unidirectional fringe patterns," Opt. Lasers Eng., 2018;106:86–93.
8. X. Yu, B. Wang, and X. Sun, "Phase unwrapping simulation of dual-frequency combined analog encoding structured light," Optik (Stuttg)., 2016;127(19): 8163–8171.
9. J. Salvi, J. Pagès, and J. Batlle, "Pattern codification strategies in structured light systems," Pattern Recognit., 2004;37(4):827–849.
10. C. Guan, L. Hassebrook, and D. Lau, "Composite structured light pattern for three-dimensional video.," Opt. Express, 2003;11(5):406–417.
11. B. Wu, T. Xue, T. Zhang, and S. Ye, "A novel method for round steel measurement with a multi-line structured light vision sensor," Meas. Sci. Technol.,2010; 21(2).
12. Y. Long, S. Wang, and W . Wu, "Robust and ef fi cient decoding scheme for line structured light," Opt. Lasers Eng., 2015;75: 88–94.
13. Z. Zhang and S. Member, "A Flexible New Technique for Camera Calibration ," 2000;22 (11):1330–1334
14. Z. Wei, C. Li, and B. Ding, "Optik Line structured light vision sensor calibration using parallel straight lines features," Opt. - Int. J. Light Electron Opt., 2014;125(17):4990–4997

15. “Measuring Planar Objects with a Calibrated Camera - MATLAB & Simulink.” 2024 Available from:http//www.mathworks.com/.
16. T. Hong, C. Rasmussen, and T. Chang, “Road Detection and Tracking for Autonomous Mobile Robots,” 2002;4715:311–319
17. P.Zanuttigh, G.Marin and C. Dal, "Time-of-Flight and Structured Light Depth Cameras" 2016
18. G. X. Ritter and J. N. Wilson, "Computer Vision Algorithms in Image Algebra in second edition". 2001.